Lab on a Chip

COMMUNICATION

View Article Online
View Journal

Cite this: DOI: 10.1039/c8lc00794b

Received 1st August 2018,
Accepted 6th September 2018

DOI: 10.1039/c8lc00794b

rsc.li/loc

Diffusion–reaction kinetics of microfluidic amperometric biosensors†

Hui Li,[a] Yi Lu[a] and Pak Kin Wong *[ab]

Amperometric biosensors are widely applied for rapid biomarker detection in physiological and environmental samples. The dynamics and linearity of the current signal, however, are only partially understood. This study investigates the diffusion–reaction kinetics of amperometric biosensing using a self-assembled monolayer (SAM) based biosensor for bacterial 16S rRNA. A numerical model is developed to optimize the chamber dimensions and elucidate the concentration dependences of the biosensor. The results revealed that depletion of substrates associated with the chamber dimension can limit the current signal in a target concentration dependent manner. This study provides practical guidelines in the design and interpretation of microfluidic amperometric biosensors for biochemical applications.

Enzymatic biosensors based on amperometric readouts can detect molecular targets, such as nucleic acids, protein, and metabolites for clinical diagnosis, the food industry, and environmental monitoring. Advances in microelectronics improve the cost-effectiveness, portability, and robustness of electrochemical biosensing systems, which facilitate their implementation in point-of-care and field-forward settings.[1,2] Furthermore, the advent of nanotechnology dramatically enhances the performance of amperometric biosensors by optimizing the immobilization strategy and reducing non-specific binding.[3] For instance, a self-assembled monolayer (SAM) based nucleic acid biosensor for bacterial 16S rRNA has been reported for rapid quantification of pathogens in patient samples at clinically relevant concentrations.[4,5] The amperometric biosensing platform can be modified for multiplex detection of protein and nucleic acid biomarkers simultaneously as well as performing pathogen identification and antimicrobial susceptibility testing.[6–8] These biosensors have also been implemented in microfluidic formats to facilitate automated analysis and point-of-care applications.[9,10]

In SAM-based amperometric biosensors, enzymes, such as horseradish peroxidase (HRP), are immobilized on the electrode surfaces using a sandwich based binding strategy (Fig. 1A). The enzyme catalyzes the reaction and creates a current readout, which can be detected amperometrically. In the amperometric biosensor for bacteria detection, a biotinylated capture probe is immobilized on the SAM on the electrode surface. The capture DNA probe binds the target 16S rRNA, which is hybridized with a fluorescein-labeled detector probe. The presence of a target 16S rRNA then immobilizes HRP conjugated with an anti-fluorescein antibody. The current obtained through the redox reaction between the substrates, including hydrogen peroxide (H_2O_2) and 3,3′,5,5′-tetramethylbenzidine (TMB), correlates with the enzyme, *i.e.*, the target 16S rRNA, captured on the electrode surface (Fig. 1B). Owing to the consumption of the substrates in the reaction, spatial concentration gradients of the substrates are created near the electrode surface and the amperometric biosensor creates a time dependent current signal.[11]

To study factors that influence the current signal, the amperometric biosensor was applied to detect the 16S rRNA of uropathogenic *Escherichia coli* (*E. coli*) from patient samples (ESI†). The concentration of the bacteria was between 10^4–10^6 cfu mL^{-1}, which covers the clinically relevant range for urinary tract infection diagnostics. The bacteria were lysed and the species-specific bacterial 16S rRNA molecules were detected using the sandwich hybridization scheme (Fig. 1B). The signal was recorded from 0 to 60 seconds (Fig. 1C). In the experiment, a rapid decay of the current was observed initially. The current signal reached a quasi-steady state in approximately 10 seconds.[4,5,9,10] It should be noted that the current continued to decrease but at a much lower rate. Fig. 1D shows the current signal at 60 seconds as a function of the target concentration. Fitting the data with the power law revealed a power exponent of 0.90 ± 0.25 and linear regression

[a] *Department of Biomedical Engineering, The Pennsylvania State University, University Park, PA, USA. E-mail: pak@engr.psu.edu*
[b] *Department of Mechanical Engineering and Department of Surgery, The Pennsylvania State University, University Park, PA, USA*

† Electronic supplementary information (ESI) available: Supplementary figure, materials, and movies of diffusion–reaction kinetics of amperometric biosensors. See DOI: 10.1039/c8lc00794b

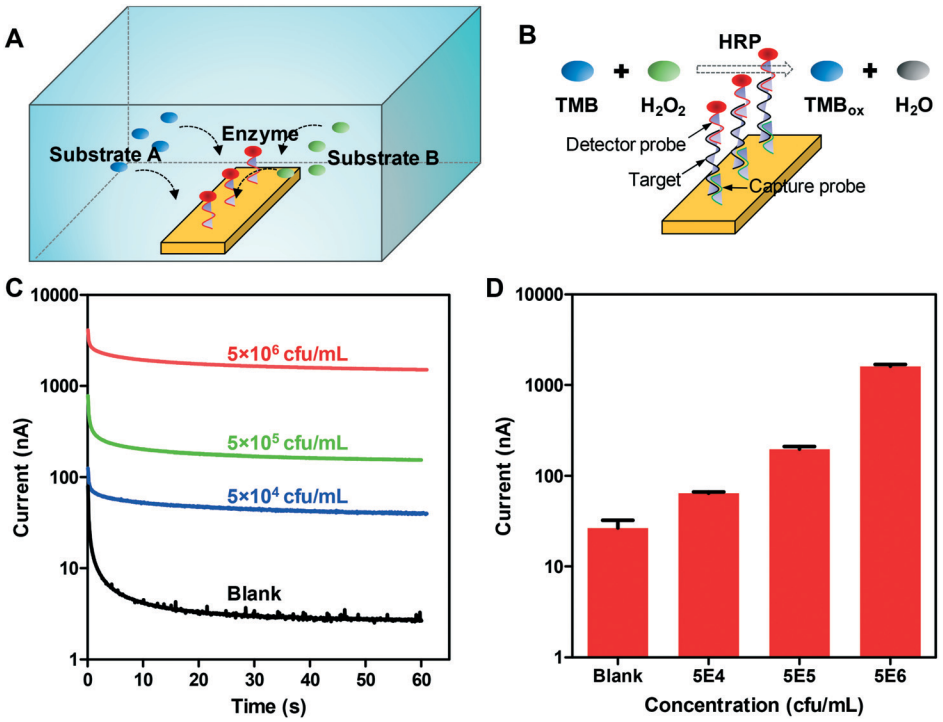

Fig. 1 An amperometric biosensor for pathogen diagnosis. (A) Schematic view of a surface reaction and diffusion model in a biosensor. (B) Molecular sensing target in a TMB–H_2O_2–HRP system. The target can be quantitatively detected by the amount of HRP that is functionalized on capture probes, which is hybridized with target and detector probes. (C) The real-time detection of *Escherichia coli* (*E. coli*) on the biosensor. (D) Representative current for different pathogen concentration at 60 s (n = 2 independent experiments, mean ± SD).

analysis revealed an R-square value of 0.9958, suggesting the relationship is approximately linear. The concentration of the bacteria was between 10^4–10^6 cfu mL^{-1}, which covers the clinically relevant range for urinary tract infection diagnostics. The limit of detection of the assay was 4.58×10^4 cfu mL^{-1} based on three times the standard deviation above the background. The value matches the clinical cutoffs for urinary tract infection diagnostics. These data illustrate the applicability of the amperometric biosensor for detecting bacterial pathogens and highlight the dynamic nature of the current signal.

A finite element model was established to study the diffusion–reaction kinetics of the amperometric biosensor (Movies S1–S3†). In the simulation, the substrate concentration was

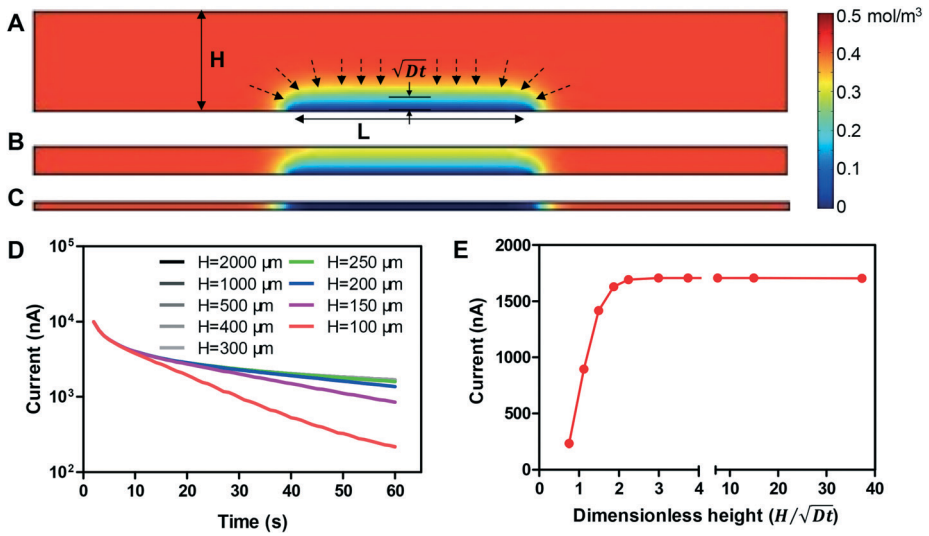

Fig. 2 Diffusion–reaction kinetics in microfluidic chambers. (A–C) The substrate (*i.e.*, TMB) distribution in sensors with height of 1000, 300, and 100 μm, respectively. The time was at 60 s. (D) Real-time detection of target in sensors with a large range height. (E) The relationship between the dimensionless height and the detection current. The target concentration was 5×10^8 cfu mL^{-1}.

uniform at the beginning of the simulation. The enzymatic reaction occurred only at the electrode surface with immobilized HRP. As the reaction proceeded, the substrates were consumed at the electrode surface. Similar to the experiment, a rapid decay of the current signal was observed in the first 10 seconds. Replenishment of the substrate by diffusion then stabilized the concentration. A depletion region was created and the distribution reached a quasi-steady state. The depletion region was approximately 300 μm above the sensor surface. Fig. 2A shows the distribution of the substrate at 60 s. As the reaction continued near the electrode surface, a quasi-steady current was generated. The time dependent signal was consistent with the experimental result, supporting that the current is governed by the diffusion–reaction kinetic of the substrate.

The amperometric biosensors have been applied in microfluidic formats for point-of-care diagnostic applications.[9,10] We therefore investigated the effect of the reaction chamber dimension on the current signal. The height of the chamber was adjusted from 2 mm to 100 μm to study the effects of the chamber dimension on the diffusion–reaction kinetics. These values were chosen to cover the length scale of typical biosensing systems, spanning from multiwell plates to microfluidic channels. Fig. 2A–C show the spatial distributions of the substrate at 60 seconds in chambers with heights of 1000, 300, and 100 μm. For chambers with a large height (*e.g.*, 1000 μm), a depletion region was created and the substrates were able to diffuse to the sensor surface from different directions (Fig. 2A). For smaller chambers (*e.g.*, 100 μm and 300 μm), the substrate was depleted in the top region and the substrate was mainly diffused from the sides (Fig. 2B and C). The time-dependent current signals were studied in chambers with various dimensions (Fig. 2D). The time-dependent current was indistinguishable for chambers with a height over 300 μm. Similar to experimental results (Fig. 1C), the real-time current reached a quasi-steady for these chambers. For smaller chambers (below 300 μm), the current signals were similar for all chambers initially (~7 seconds). After the initial period, the current signal displayed a dimension dependence and generally decreased with the chamber size. In these cases, the current did not reach a quasi-steady state. The discrepancy was attributed to the substrate depletion in the top region of the chamber, which extended toward two sides of the chamber (*e.g.*, Fig. 2C)

The current signal was plotted as a function of the dimensionless height (Fig. 2E). In this study, the dimensionless height was the ratio between the chamber height, H, and the diffusion length, L. The diffusion length was calculated by the diffusion coefficient and the reaction time ($L = \sqrt{Dt}$). The dimensionless height, H/L, is related to the mass Fourier number, $Fo_m = Dt/H^2$, and is associated with the depletion length in the quasi-steady state.[12] In the numerical analysis, the current increased linearly with the dimensionless height and reached a plateau when the dimensionless height is approximately 2. Further increase in the chamber height did not have a significant effect on the current signal. In other words, the height of the reaction chamber should be significantly larger than the diffusion length to avoid the signal reduction due to substrate depletion in the top region of the reaction chamber.

We further investigated the effect of target (and enzyme) concentration, which directly determines the reaction kinetics on the sensor surface, on the current signal. It is important to evaluate the nonlinearity related to the target concentration as amperometric biosensors are applied for detecting various analytes with a large concentration range. Fig. 3A–C show the substrate distribution in a reaction chamber with a height of 300 μm at 60 s. The target concentrations were 1.0×10^8, 1.0×10^6, and 1.0×10^4 cfu mL^{-1}. These values were equivalent to concentrations from nanomolar to sub-picomolar. Examining the results revealed that the chemical gradient decreased with the target concentration and the depletion region was not observable at low target concentrations (*e.g.*, 1.0×10^4 cfu mL^{-1} or below). The current was calculated as a function target concentration (Fig. 3D). At a low target concentration, the current increased linearly with the concentration and was consistent with experimental results (Fig. 1D). This assumption is valid when the current is reaction rate limited. At a high concentration, the current was limited due to the diffusion of substrates and the signal displayed nonlinearity relative to the target concentration. The threshold concentration for the transition was at approximately 10^6 cfu mL^{-1} in the current biosensor condition.

To generalize the result, we analyzed the effects of dimensionless height and target concentration on the signal of the amperometric biosensor (Fig. 3E). At low target concentrations (*e.g.*, below 1.0×10^6 cfu mL^{-1}), the current at the quasi-steady state increased linearly with the target concentration and was independent of the chamber dimension, as the reaction was reaction rate limited. This linearity is a typical assumption in the interpretation of amperometric biosensors. Nevertheless, the numerical results suggest the current response could be limited by the target concentration. This nonlinear response is important when the dimension of the reaction chamber is comparable to the diffusion length of the substrates (*e.g.*, in microfluidic systems). For instance, the current signal displayed a high nonlinearity between 10^6 and 10^9 cfu ml^{-1} when the dimensionless height is 1. A maximum was observed at 10^7 cfu mL^{-1} and the current decreased with high target concentration due to the depletion of the substrate (Fig. 3E and S1†).

This study reports an integrated experimental and computational investigation of the dynamics and linearity of amperometric biosensors. The biosensor detects bacterial 16S rRNA and exhibits a linear response from 10^4 to 10^6 cfu mL^{-1}, which allows diagnosis of urine tract infections. To understand the performance of the biosensor, a numerical model was built based on a simplified geometry. Convection and sources of noise within the chambers were ignored. Despite the simplified assumptions, the

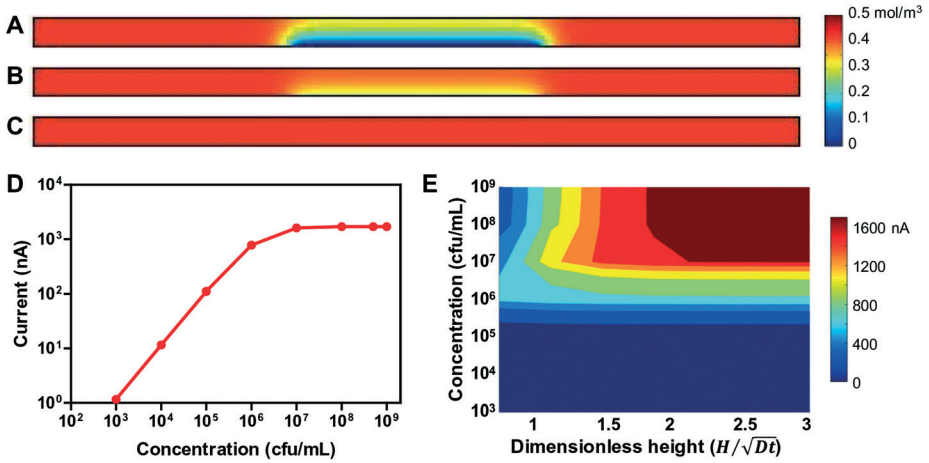

Fig. 3 Dimension and concentration dependences of amperometric biosensors. (A–C) The substrate distribution in the sensor with target concentration of 1×10^8, 1×10^6, and 1×10^4 cfu mL^{-1}, respectively. The sensor height was 300 μm and the time was at 60 s. (D) The dynamic range of pathogen diagnosis was studied for the sensor at height of 300 μm. (E) The dynamic range of pathogen diagnosis was studied for sensors with different dimensions.

model successfully captured the essence of the current signal observed in the experiment. While the initial current is proportional to the enzyme concentration, the current signal is typical measured at the quasi-steady state to minimize the uncertainties due to substrate loading time and motion of the substrate solution. At the quasi-steady state, the current is governed by the local concentration of the substrate. Our results revealed a nonlinearity of amperometric biosensors that is associated with the dimension of the reaction chamber. In particular, the current signal can be limited by the dimension of the reaction chamber and the target concentration in an interrelated manner. Microfluidic amperometric biosensors for bacterial 16S rRNA are known to have a lower signal level compared to the manual assay with a large dimension.[9,10] Furthermore, amperometric biosensors are saturated at high target concentrations.[13] Our model provides a physical explanation that contributes to the reduction in the current signal in these studies. Importantly, the results will represent useful guidelines in the design and interpretation of the microfluidic biosensors with amperometric readouts in the future.

Conclusions

This study investigates the diffusion–reaction kinetics of amperometric biosensors. Our results reveal a nonlinearity of the sensing scheme associated the reaction chamber dimension and provide guideline in the implementation of microfluidic electrochemical biosensors.

Conflicts of interest

There are no conflicts to declare.

Acknowledgements

The authors thank for Dr. Jian Gao for insightful discussion.

Notes and references

1 M. L. Sin, J. Gao, J. C. Liao and P. K. Wong, *J. Biol. Eng.*, 2011, **5**, 6.
2 G. Whitesides, *Lab Chip*, 2010, **10**, 2317–2318.
3 T. Wink, S. J. van Zuilen, A. Bult and W. P. van Bennkom, *Analyst*, 1997, **122**, 43R–50R.
4 E. M. K. Kurundu Hewage, D. Spear, T. M. Umstead, S. Hu, M. Wang, P. K. Wong, Z. C. Chroneos, E. S. Halstead and N. J. Thomas, *SLAS Technol.*, 2017, **22**, 616–625.
5 J. Gao, L. Jeffries, K. E. Mach, D. W. Craft, N. J. Thomas, V. Gau, J. C. Liao and P. K. Wong, *SLAS Technol.*, 2017, **22**, 466–474.
6 E. Altobelli, R. Mohan, K. E. Mach, M. L. Y. Sin, V. Anikst, M. Buscarini, P. K. Wong, V. Gau, N. Banaei and J. C. Liao, *Eur. Urol. Focus*, 2017, **3**, 293–299.
7 T. Liu, M. L. Sin, J. D. Pyne, V. Gau, J. C. Liao and P. K. Wong, *Nanomedicine*, 2014, **10**, 159–166.
8 T. Liu, Y. Lu, V. Gau, J. C. Liao and P. K. Wong, *Ann. Biomed. Eng.*, 2014, **42**, 2314–2321.
9 M. L. Sin, V. Gau, J. C. Liao and P. K. Wong, *J. Microelectromech. Syst.*, 2013, **22**, 1126–1132.
10 M. Ouyang, R. Mohan, Y. Lu, T. Liu, K. E. Mach, M. L. Sin, M. McComb, J. Joshi, V. Gau, P. K. Wong and J. C. Liao, *Analyst*, 2013, **138**, 3660–3666.
11 T. M. Squires, R. J. Messinger and S. R. Manalis, *Nat. Biotechnol.*, 2008, **26**, 417–426.
12 S. K. Das, *Fundamentals of heat and mass transfer*, Alpha Science International, Oxford, U.K., 2010.
13 K. E. Mach, R. Mohan, E. J. Baron, M. C. Shih, V. Gau, P. K. Wong and J. C. Liao, *J. Urol.*, 2011, **185**, 148–153.

